Available online at www.sciencedirect.com
ScienceDirect
Ceramics International 35 (2009) 221–227
CERAMICS INTERNATIONAL
www.elsevier.com/locate/ceramint

Microstructural and electrical behavior of $Bi_4V_{2-x}Cu_xO_{11-\delta}$ ($0 \leq x \leq 0.4$)

Ravi Kant, K. Singh, O.P. Pandey *

School of Physics and Materials Science, Thapar University, Patiala 147004, India

Received 19 July 2007; received in revised form 28 August 2007; accepted 4 October 2007
Available online 4 February 2008

Abstract

Cation substituted bismuth vanadate possesses high oxygen ion conductivity at lower temperatures. The ionic conductivity of this material at 300 °C is 50–100 times more than any other solid electrolyte. Three phases (α, β, γ) are observed in the substituted compound; α and γ are low and high conducting phase, respectively. Samples of $Bi_4V_{2-x}Cu_xO_{11-\delta}$ ($x = 0$–0.4) were prepared by solid-state reaction technique. Impedance spectroscopy measurements were carried out in the frequency range of 100 Hz to 100 kHz using gold sputtered cylindrical shaped pellets to obtain bulk ionic conductivities as a function of the substitution and temperature. The change of slopes observed in the Arrhenius plots is in agreement with the phase transitions for all the compositions. The highest ionic conductivity of the Cu-substituted compound was observed in $Bi_4V_{1.8}Cu_{0.2}O_{11-\delta}$ which is attributed to its lower activation energy. Microstructural studies indicated the stabilization of high temperature γ-phase at low temperature in those samples whose ionic conductivity observed was higher.

Keywords: A. Sintering; B. Grain growth; C. Ionic conductivity; D. X-ray diffraction

1. Introduction

$Bi_4V_2O_{11-\delta}$ electrolytes exhibit high ionic conductivity at moderate temperature range (600–800 °C) as compared to other reported solid electrolytes [1–5]. It is currently under intensive study to optimize their properties as an electrolyte for solid oxide fuel cells applications [6–9]. The ionic conductivity of these systems can be enhanced by two ways, viz., phase transition and increasing disordering in the system by doping of various cations. On the basis of electrical studies [10] and structure, various models for ionic conduction based on the defect structure are proposed [11–13]. Basically, bismuth vanadate exhibits Aurivillius layered perovskite structure with $[Bi_2O_2]_n^{2n+}$ and $[VO_{3.5}\square_{0.5}]$ perovskite layers alternatively. $[VO_{3.5}\square_{0.5}]$ layers contain random oxide ion vacancy □ and substitution of V by different cations that results in an increase in vacancy concentration in the vanadate layer. The environment of vanadium in α-$Bi_4V_2O_{11}$ was investigated by nuclear magnetic resonance (NMR) studies [14]. The $Bi_4V_2O_{11}$ exhibits three polymorphs due to long-range vacancy ordering with the transition temperatures of $\alpha \leftrightarrow \beta$ and $\beta \leftrightarrow \gamma$ at about 420 °C and 570 °C, respectively. However, substitution of isovalent or aliovalent cations, e.g. Cu, Ti, Al, Mn, etc. for V can suppress the transitions and stabilize the high temperature γ-phase at room temperature [15–18]. Structural, thermal, electrical characterizations and their correlation with the conduction mechanism of $Bi_4V_{1.9}Cu_{0.1}O_{11-\delta}$ have already been reported by other researchers [19–22]. But so far, no detailed study on compositional variation beyond 10% doping of copper and DSC studies up to their melting points have been reported. Moreover, microstructural studies of these transitions have not yet been studied.

In the present investigation, samples of the series of $Bi_4V_{2-x}Cu_xO_{11-\delta}$ ($0 \leq x \leq 0.4$) named as BICUVOX have been prepared by solid-state reaction method. These samples are characterized by XRD, DSC and ac conductivity measurements.

Although, a number of studies have been reported aimed specifically at establishing relation between phase stability and ionic conductivity of the BIMEVOX system but no report exist to correlate them with microstructure. The basic aim of the present work is to correlate the microstructural changes with ionic conductivity of the above series.

* Corresponding author. Tel.: +91 175 2393116; fax: +91 175 2393005.
E-mail addresses: ravikant_mail@rediffmail.com (R. Kant), ksbadla@yahoo.co.in (K. Singh), oppandey@tiet.ac.in (O.P. Pandey).

0272-8842/$34.00
doi:10.1016/j.ceramint.2007.10.020

2. Experimental techniques

$Bi_4V_{2-x}CuO_{11-\delta}$ ($0 \leq x \leq 0.4$) powders were prepared by solid-state reaction from stoichiometric amounts of the following oxides: Bi_2O_3 (99%), V_2O_5 (99%), and CuO (99.99%). The starting powders were mixed in acetone media in mortar pestle for an hour to break any large agglomerates. The mass was subsequently ball milled for 2 h to achieve a fully homogeneous powder mixture. The resulting powders were dried and thoroughly ground and then fired at 700 °C in silica crucibles for 12 h in air. Calcined powders were ground, mixed and refired at 800 °C for 12 h. The sintered powders were further ground and compacted at a pressure of 98,000 N after mixing with a 10% poly vinyl alcohol (PVA) binder to make pellets of approximately same dimensions. The so prepared pellets were sintered at optimum temperature of 800 °C for 10 h. The X-ray diffractograms of the samples of the pellets of different compositions were obtained by Rigaku (Model Geiger flex) in the scan speed of 5°/min. Differential scanning calorimetric (DSC) measurement was performed by Perkin Elmer at the heating rate of 20 °C/min in nitrogen atmosphere. Ionic conductivity was measured by an ac impedance spectroscopy with Model 4274 A multi-frequency Hewlett-Packard LCR meter in the frequency range of 100 Hz to 100 kHz using two probe technique. The gold sputtered pellets were used to carry out ac conductivity measurement in the temperature range of 200–700 °C during cooling cycle.

3. Results and discussion

X-ray diffraction (XRD) pattern of $Bi_4V_{2-x}Cu_xO_{11-\delta}$ ($x = 0$ and $x = 0.1$) exhibit orthorhombic structure. However, higher concentration of Cu-doping in $Bi_4V_{2-x}O_{11-\delta}$ leads to phase transition from orthorhombic (α) to tetragonal (γ) phase which is in good agreement with the earlier reported work [23,24]. The typical XRD patterns observed for $Bi_4V_{2-x}Cu_xO_{11-\delta}$ ($0 \leq x \leq 0.4$) are shown in Fig. 1. The XRD pattern of pure $Bi_4V_{2-x}O_{11}$ and Cu = 0.1 shows very weak reflections at $2\theta \approx 24.18°$ and 24.12° which is attributed to superstructure of α-form as has also been reported in the literature [25]. It clearly indicates that samples of $x = 0$ and $x = 0.1$ exhibit orthorhombic structures.

Apart from this, samples of $Bi_4V_{2-x}Cu_xO_{11-\delta}$ ($0.1 \leq x \leq 0.4$) also exhibit some extra peaks. These peaks may be attributed to Bi_2O_3 and are shown in XRD pattern (Fig. 1). Another extra peak for Bi_2O_3 at $2\theta = 27.32°$ is overlapping with the $Bi_4V_{2-x}Cu_xO_{11-\delta}$ phase for $x = 0.1$ and 0.2 whereas it has been identified for $x = 0.3$ and 0.4. In earlier studies, Reiselhuber *et al.* [26] and Huve *et al.* [27] reported some extra peaks in similar compound which are due to $BiVO_4$.

Comparison of XRD patterns of samples of $x = 0$ and $x = 0.1$ do not show any significant change in their *d*-values except some peak broadening. This may be attributed to disorder enhancement with in $x = 0.1$ sample as compared to $x = 0$ sample with lattice parameters: $a = 5.52$ Å, $b = 5.6$ Å, $c = 15.24$ Å and $a = 5.51$ Å, $b = 5.60$ Å, $c = 15.28$ Å, respectively. The change in c-direction lattice parameter is due to size

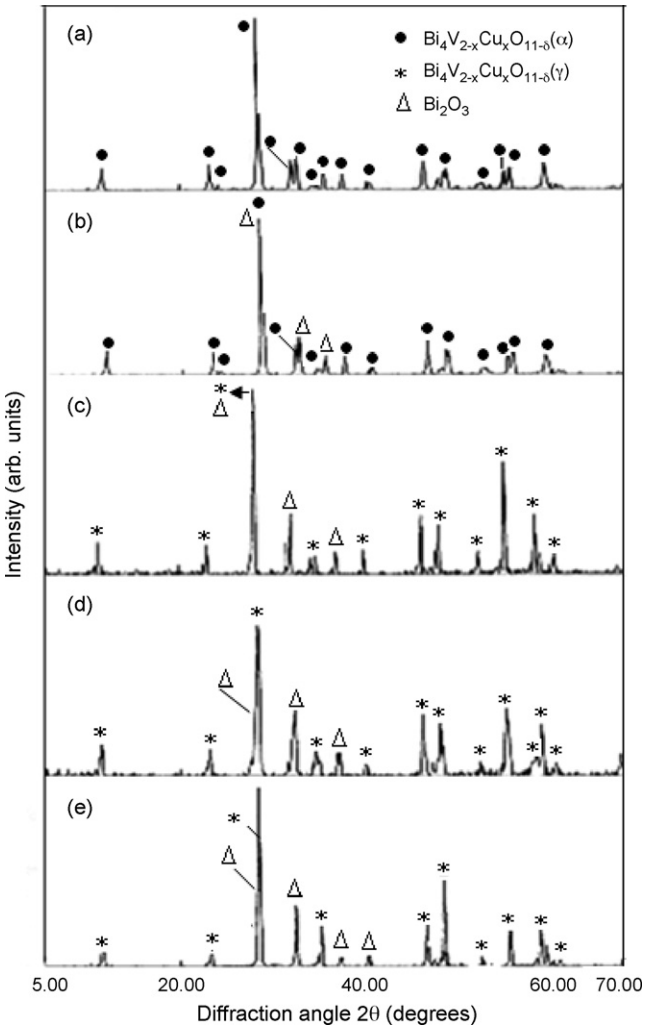

Fig. 1. XRD pattern of $Bi_4V_{2-x}Cu_xO_{11-\delta}$: (a) $x = 0$, (b) $x = 0.1$, (c) $x = 0.2$, (d) $x = 0.3$ and (e) $x = 0.4$.

difference between Cu^{2+} and V^{5+} and Cu may occupy the site along c-direction.

In contrast to these, XRD patterns of $x = 0.2$, 0.3 and 0.4 clearly indicate the shifting of peaks at lower diffraction angle. It is due to phase transition of α to γ at room temperature. Interestingly, these X-ray pattern could not exhibit the doublets at $2\theta \approx 31°$, 39°, 48° and 54° as observed in $x = 0$ and 0.1 samples which are characteristic of α-super structure lattice. The graphical variation of lattice parameters for tetragonal γ-phase $0.2 \leq x \leq 0.4$ is shown in Fig. 2.

The two-phase transitions corresponding to $\alpha \rightarrow \beta$ and $\beta \rightarrow \gamma$ are evident in the sample of $x = 0$ at 450 °C and 520 °C whereas transition corresponding to $\beta \rightarrow \gamma$ is suppressed by partial substitution of copper for vanadium in $Bi_4V_2O_{11}$. The transition corresponding to $\alpha \rightarrow \gamma$ at 480 °C for $x = 0.1$ as shown in Arrhenius plot (Fig. 3) which is in good agreement with the DSC measurement in which two endothermic transitions are observed at 453 °C and 520 °C for $x = 0$ and one transition for $x = 0.1$ at 480 °C (Fig. 4). However, samples of $x = 0.1$ and $x = 0.2$ exhibit additional exothermic transitions at 725 °C, respectively which may be attributed due to

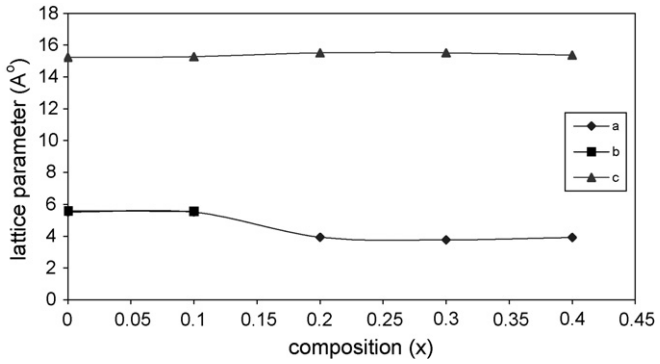

Fig. 2. Composition vs. lattice parameter of $Bi_4V_{2-x}Cu_xO_{11-\delta}$ ($0 \le x \le 0.4$).

unreacted Bi_2O_3 tranforming to δ-Bi_2O_3 phase at 725 °C in these samples. α-Bi_2O_3 at room temperature exhibit monoclinic structure and transform to δ-FCC structure at 727 °C as has been reported by Yaremchenko *et al.* [28]. The XRD patterns of these samples (Fig. 1) also exhibited weak reflection indexed to Bi_2O_3. When the Cu content increases, the unreacted-Bi_2O_3 portion also increases. Further, increase in doping of Cu^{2+} for V^{5+} may occupy some sites even in Bi_2O_3 which results in very weak (sluggish) exothermic peak at lower temperature than $x = 0.1$ and $x = 0.2$ samples as shown in Fig. 4. In $x = 0.4$ sample, the DSC curve clearly indicates two endothermic peaks at 780 °C and 875 °C apart from a peak at 532 °C ($\gamma \rightarrow \gamma'$ transition), which belongs to melting of Bi_2O_3 and γ-$Bi_4V_2O_{11}$, respectively.

Enhancement of conductivity for 5% copper substitution on vanadium sites due to oxygen vacancies in $Bi_4V_2O_{11}$ compound is shown in Arrhenius plot (Fig. 3).

However, XRD pattern of both the samples are same. It means the enhancement in conductivity of these samples is essentially due to disordering instead of γ-phase stabilization at room temperature. However, in case if phase transition is occurring then the volume of transformed phase is less than the sensing limit of the X-ray diffraction range. In order to provide further support to this hypothesis, the microstructures of these samples are taken at same magnifications which are shown in Fig. 5. The scanning electron micrographs (SEM) of fractured surface of $x = 0$ and $x = 0.1$ do not show any significant change except larger grain size in case of $x = 0.1$ sample with little higher porosity. On careful examination of micrographs for both the samples ($x = 0$ and $x = 0.1$) in Fig. 5, one can see the

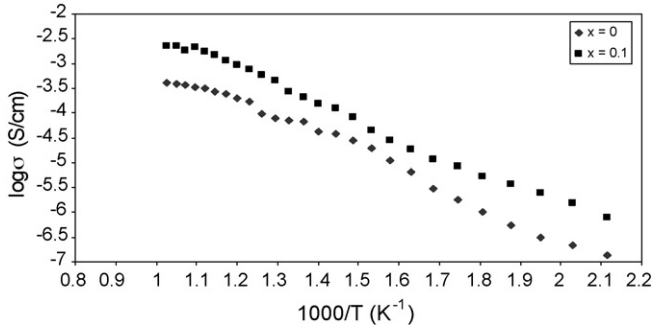

Fig. 3. Conductivity measurement of $Bi_4V_{2-x}Cu_xO_{11-\delta}$ (pure and $x = 0.1$).

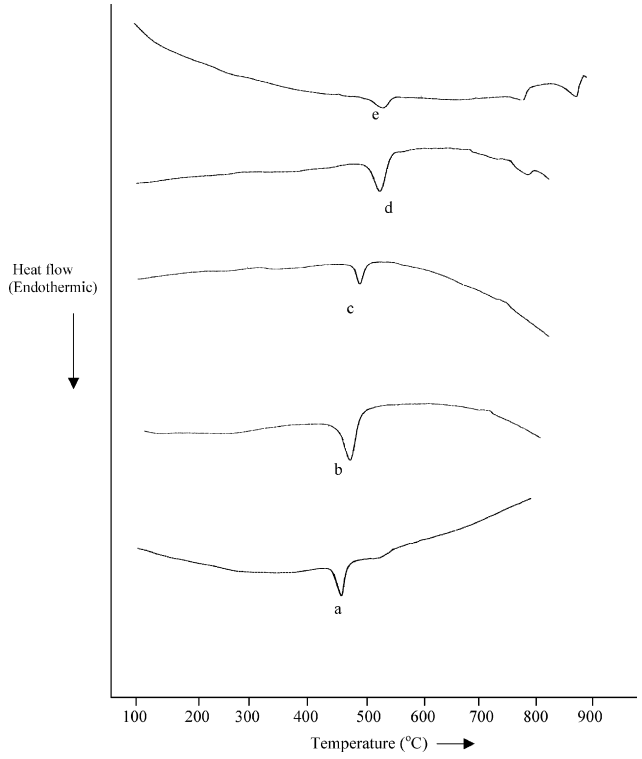

Fig. 4. DSC plot of $Bi_4V_{2-x}Cu_xO_{11-\delta}$ (a) $x = 0$, (b) $x = 0.1$, (c) $x = 0.2$, (d) $x = 0.3$ and (e) $x = 0.4$.

interwoven wavy network (marked as arrow in the Fig. 5) type of structure existing throughout the sample. Though the volume fraction of this network structure of lamellar type is more for sample $x = 0$ as compared to $x = 0.1$ but in both cases it is uniformly distributed throughout the sample. This type of structure in ceramic compounds has been reported for piezoelectric materials [29,30]. During sintering, the substance crystallizes above Curie temperature in the cubic perovskite structure and transforms in to lower symmetry structure during cooling. The phase transformation leads to lattice distortion. Due to lattice distortion, thermal stresses are generated which are further reduced by the formation of domains. The domain configuration consists of 90° and 180° domains. Based on the different possibilities of their orientation and with variation in crystal structure, these orientations may also change. Since we are analyzing the fractured surface so instead of parallel straight lines, we are observing a parallel wavy pattern. But it is certain that the structure comprises of these parallel domains which form because of thermal lattice strain during cooling after sintering. The other variation in structure for sample ($x = 0.1$) as compared to ($x = 0$) is that at certain places where the grain growth is more pronounced, open and continuous pores along the grain boundary can be seen. This further support our argument that since no phase transformation is observed in X-ray analysis but enhanced conductivity is observed because of the fact that there is a thermal mismatch between the high temperature γ-phase which transforms to α-phase at room temperature but even at room temperature γ-phase exists. The shining grains of bigger size with black appearances correspond to γ-phase around which the bigger continuous pores are

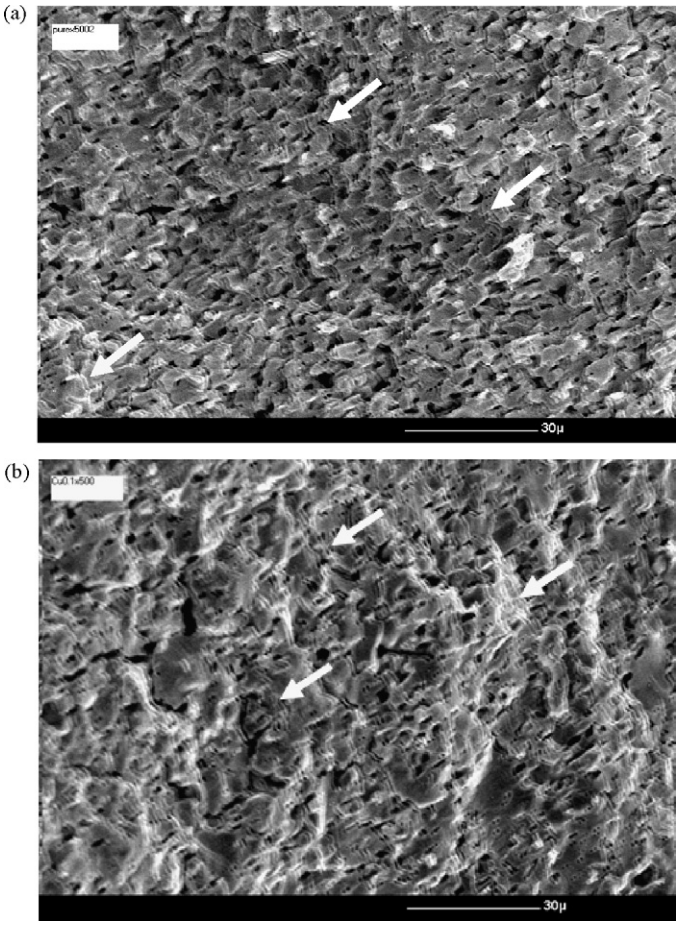

Fig. 5. SEM photograph of fractured surface of: (a) Cu = 0 and (b) Cu = 0.1.

observed. Since volume fraction of this room temperature stabilized γ-phase is very less so X-ray is unable to detect it. The conclusion drawn from above analysis is that the doped sample ($x = 0.1$) leads to higher ionic conductivity because of this, room temperature stabilized γ-phase which is less as compared to α-phase ($x = 0$).

In contrast to these, the $0.2 \leq x \leq 0.4$ samples show totally different microstructures than $x = 0$ and $x = 0.1$ samples (Fig. 6) which is due to γ-phase stabilization. In these microstructures, the grains are very large and their size increases with impurity concentration. The SEM observation of the fractured surface shows that the addition of CuO for $x = 0.2$ substitution and beyond has a strong effect on the microstructure and grain growth of $Bi_4V_2O_{11}$. The higher ionic conductivity for Cu = 0.2 in $Bi_4V_{2-x}Cu_xO_{11-\delta}$ is further supported by the more uniformity in grains pattern and size with lesser porosity as compared to Cu = 0.3 and 0.4.

However, for sample containing more than $x = 0.2$, there is no wavy pattern observed indicates that even at room temperature, the high temperature γ-phase gets stabilized. The ordering of the oxygen vacancies in α- and β-phase in $Bi_4V_{2-x}Cu_xO_{11-\delta}$ leads to a drop in conductivity. Partial substitution of vanadium by copper prevents this ordering and allows stabilization of the high symmetry γ-$Bi_4V_2O_{11}$ phase. The slightly higher slope of the Arrhenius plot in the low

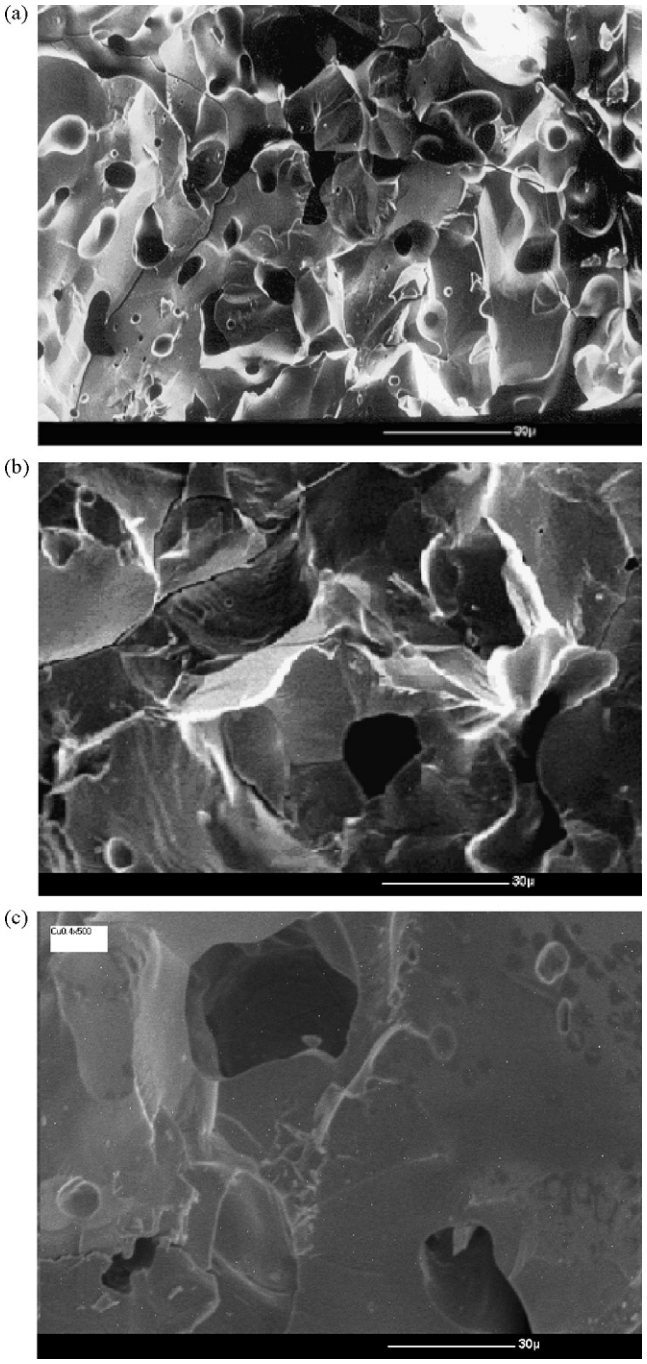

Fig. 6. Fractured surface SEM photographs of: (a) Cu = 0.2 (b) Cu = 0.3 and (c) Cu = 0.4.

temperature range (Fig. 7) is probably associated with the incommensurable modulation of the structure. In these particular samples ($x = 0.2$, 0.3 and 0.4), the cell parameters 'c' increases while, the 'a' parameter and unit cell volume of tetragonal γ-$Bi_4V_{2-x}Cu_xO_{11-\delta}$ decreases with Cu up to $x = 0.3$ as shown in Table 1 because, an increase of vacancy content is expected to decrease unit cell size which is in good agreement with the trend of decreasing volume with increasing oxygen vacancy contents as also corroborated by Yan *et al.* [31] for the titanium substitution in the same composition range where as the both 'a', 'c' parameters and volume varies in reverse order

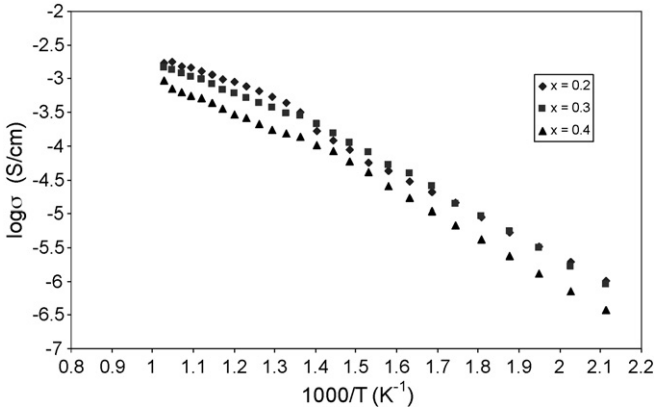

Fig. 7. Conductivity of $Bi_4V_{2-x}Cu_xO_{11-\delta}$ ($0.2 \leq x \leq 0.4$).

Table 1
The unit cell parameters of γ-$Bi_4V_{2-x}Cu_xO_{11-\delta}$

Composition	a (Å)	c (Å)	Volume (Å)
$x = 0.2$	3.94	15.51	240.77
$x = 0.3$	3.77	15.52	220.58
$x = 0.4$	3.93	15.38	237.54

from $x = 0.3$–0.4 because of larger effective ionic radius of Cu^{II} (0.72 Å) as compared with that of V^{V} (0.59 Å) which dominates the increase of oxygen vacancies possibly due to higher value of copper substitution. This is also evident in the observed lower value of ionic conductivity from $x = 0.3$ to $x = 0.4$. The decrease of densities of these samples with increasing doping of Cu for vanadium also confirms above hypothesis.

Conductivity values were extracted from impedance complex plane plots. When real part (Z') is plotted against imaginary part (Z'') at different frequencies, it gives rise to semicircle as shown in representative plot for $x = 0.3$ at room temperature (Fig. 8). From the interception of the plot on the x-axis (Z'), the true bulk resistance R can be calculated by which conductivity of the sample is measured.

The impedance spectra obtained for BICUVOX are similar to those observed for other BIMEVOXs. The general features of the impedance spectra and their evolution with temperature are similar for all of the compositions studied. For temperatures below 400 °C, the impedance spectra consisted of one semicircle. Contribution from the bulk sample and grain boundaries could not be distinguished, except a broadened semicircle with a low frequency spike. As the temperature increases, the resistance decreases and higher frequencies are required to measure complete semicircles due to total

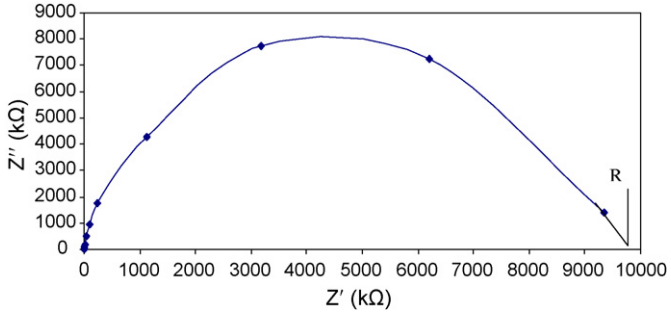

Fig. 8. Complex impedance data at room temperature of $Bi_4V_{2-x}Cu_xO_{11-\delta}$ ($x = 0.3$).

conductivity (bulk + grain boundary contributions). Since the available maximum frequency of the impedance analyzer is fixed, the semicircle corresponding to the bulk resistance may go on vanishing on the high frequency side. At the highest temperatures, a spike only at very low frequencies associated with the polarization of the electrode is observed and this suggests that the compound is primarily an ionic conductor [20,32]. The conductivity behavior of the BICUVOX ($x = 0$, $x = 0.1$) compositions generally shows three linear regions with different activation energies in their Arrhenius plots. These three regions are $\alpha \rightarrow \beta \rightarrow \gamma$ phase transitions as shown in Fig. 2.

For the linear region below 440 °C and above 540 °C, activation energy (E_a) values along with ionic conductivities at 300 °C and densities for $x = 0.2$, 0.3 and 0.4 samples are summarized in Table 2.

The higher ionic conductivity for Cu = 0.2 than Cu = 0.3 and Cu = 0.4 is in good agreement with the density calculated for all the compositions. The decrease of ionic conductivity (Table 2) with increasing oxygen vacancy concentrations can be attributed to the formation of defect pairs for x up to 0.3 and the sharp decrease of ionic conductivity for $x = 0.4$ can be due to the possibility that the true solid solution formation range of the Cu-substituted is $x < 0.4$ [31]. Some researchers have reported that unreacted CuO might have segregated along the grain boundary causing the decrease in conductivity [33,34]. In the present case, the XRD and DSC measurements indicate that instead of CuO, Bi_2O_3 segregated and this may lead to decrease the ionic conductivity of these samples.

The transitions corresponding to $\gamma \rightarrow \gamma'$ are evident in the ionic conductivity plots at 500 °C, 520 °C and 540 °C for $x = 0.2$, 0.3 and 0.4, respectively as shown in Arrhenius plot (Fig. 7). The high conducting γ-phase is attributed to its low activation energy in the two different slope regions in the Arrhenius plot of $\log \sigma$ versus $1000/T$. DSC measurements

Table 2
Conductivity, density and activation energy at different composition of $Bi_4V_{2-x}Cu_xO_{11-\delta}$

Composition	σ (S/cm) at 300 °C	E_a (eV) <440 °C	E_a (eV) >540 °C	Density (g/cc)
$x = 0.2$	1.4233×10^{-5}	0.2641	0.1567	6.50
$x = 0.3$	1.4163×10^{-5}	0.2880	0.1932	6.20
$x = 0.4$	6.7803×10^{-6}	0.3014	0.2235	6.07

for these samples (Fig. 4) also display the phase transitions at 485 °C, 520 °C and 535 °C for $x = 0.2$, 0.3 and 0.4, respectively which shows that phase transition temperature goes on increasing with dopant concentration and this further confirms the increase of ferroelectric transition and curie temperature as reported by Prasad *et al.* [35]. Slight discrepancies in the two transition temperatures for $x = 0.2$ and 0.3 by these two different measurements indicate that the structural changes involved in these transitions are sluggish [36]. Moreover for sample $x = 0.3$ and 0.4, the fractured surface micrographs show parallel wavy pattern. Though this is not that much pronounced as compared to $x = 0$ and $x = 0.1$ samples but their presence has been noticed. This typical pattern corresponds to α-phase which has low conductivity as compared to γ-phase. Whereas this type of pattern is not seen for sample of $x = 0.2$ (Fig. 6). This clearly indicate that structures where a drastic change has been observed for $x = 0.2$–0.4 as compared to $x = 0$ and $x = 0.1$ is responsible for observation of high temperature γ-phase which is stabilized at room temperature.

4. Conclusion

The high temperature, high oxide ion conducting γ-phase of $Bi_4V_2O_{11}$ is stabilized for $Bi_4V_{2-x}Cu_xO_{11-\delta}$ with $x \geq 0.2$. The highest ionic conductivity was found for the $Bi_4V_{1.8}Cu_{0.2}O_{11-\delta}$ of the substituted compounds at lower temperatures. The low values of conductivity obtained for all the compositions as compared to reported value of 1×10^{-3} at 300 °C may be attributed due the segregation of Bi_2O_3 as impurity and processing conditions. In general, at 300 °C, the $\sigma_{0.4} < \sigma_{0.3} < \sigma_{0.2}$ in the γ-phase region. The increased conductivity trend is consistent with the trend of decreased activation energy (E_a: $x = 0.4 > 0.3 > 0.2$) which is further supported by microstructural evidences.

Acknowledgement

We are very grateful to All India Council for Technical Education, New Delhi, India, for financial support to carry out above research.

References

[1] Y. Liu, L.E. Lao, Structural and electrical properties of ZnO-doped 8 mol% yttria-stabilized zirconia, Solid State Ionics 177 (1–2) (2006) 159–163.
[2] A. Rizea, D. Chirlesan, C. Petot, G. Petot-Ervas, The influence of alumina on the microstructure and grain boundary conductivity of yttria-doped zirconia, Solid State Ionics 146 (3–4) (2002) 341–353.
[3] A. Sinha, B.P. Sharma, P. Gopalan, Development of novel perovskite based oxide ion conductor, Electrochim. Acta 51 (7) (2006) 1184–1193.
[4] D.S. Lee, W.S. Kim, S.H. Choi, J. Kim, H.W. Lee, J.H. Lee, Characterization of ZrO_2 co-doped with Sc_2O_3 and CeO_2 electrolyte for the application of intermediate temperature SOFCs, Solid State Ionics 176 (1–2) (2005) 33–39.
[5] D.S. Lee, J.W. Heo, J.D. Kim, J.S. Kim, H.W. Lee, G.H. Kim, D.J. Kim, J.H. Lee, Electrical conductivity of ZrO_2 doped with Sc_2O_3 and CeO_2, J. Korean Ceram. Soc. 39 (4) (2002) 346.
[6] N.Q. Minh, Ceramic fuel cells, J. Am. Ceram. Soc. 76 (3) (1993) 563–588.
[7] A.J. Feighery, J.T.S. Irvine, Effect of alumina additions upon electrical properties of 8 mol% yttria-stabilised zirconia, Solid State Ionics 121 (1999) 209–216.
[8] J.A. Kilner, Fast oxygen transport in acceptor doped oxides, Solid State Ionics 129 (2000) 13–23.
[9] O. Yamamoto, Solid oxide fuel cells: fundamental aspects and prospects, Electrochim. Acta 45 (15) (2000) 2423–2435.
[10] F. Krok, I. Abraham, M. Malys, W. Bogusz, J.R. Dygas, J.A.G. Nelstrop, A.J. Bush, Structural and electrical consequences of high dopant levels in the BIMGVOX system, Solid State Ionics 136/137 (2000) 119–125.
[11] I. Abraham, F. Krok, A model for the mechanism of low temperature ionic conduction in divalent-substituted γ-BIMEVOXes, Solid State Ionics 157 (2003) 139–145.
[12] E. Capoen, M.C. Steil, N. Tancret, G. Nowogrocki, J.C. Boivin, G. Mairesse, R.N. Vannier, M. Anne, O. Isnard, Time resolved in situ neutron diffraction investigation of the electrochemical reduction of BIMEVOX, Solid State Ionics 175 (2004) 419–424.
[13] G. Mairesse, P. Roussel, R.N. Vannier, M. Anne, G. Nowogrocki, Crystal structure determination of α-, β-, and γ-$Bi_4V_2O_{11}$ polymorphs. Part II: crystal structure of α-$Bi_4V_2O_{11}$, Solid State Sci. 5 (6) (2003) 861–869.
[14] F. Delmaire, M. Rigole, E.A. Zhilinskaya, A. Aboukais, R. Hubaut, G. Mairesse, V magic angle spinning solid state NMR studies of $Bi_4V_2O_{11}$ in oxidized and reduced states, Phys. Chem. Chem. Phys. 2 (19) (2000) 4477–4483.
[15] J.B. Goodenough, A. Manthiram, M. Paranthaman, Y.S. Zhen, Oxide ion electrolytes, Mater. Sci. Eng. B 12 (4) (1992) 357–364.
[16] V. Sharma, A.K. Shukla, J. Gopalakrishanan, Effect of aliovalent-cation substitution on the oxygen-ion conductivity of $Bi_4V_2O_{11}$, Solid State Ionics 58 (3–4) (1992) 359–362.
[17] C.K. Lee, B.H. Bay, A.R. West, New oxide ion conducting solid electrolytes, $Bi_4V_2O_{11}$:M;M=B,Al,Cr,Y,La, J. Mater. Chem. 6 (1996) 331–336.
[18] Y.L. Yang, L. Qin, W.T.A. Harrison, R. Christoffersen, A.J. Jacobson, Manganese doped bismuth vanadate solid electrolytes, J. Mater. Chem. 7 (2) (1997) 243–248.
[19] S.P. Simner, D.S. Sandoval, J.D. Mackenzie, bruce Dunn, Synthesis, densification, and conductivity characteristics of BICUVOX oxygen-ion-conducting ceramics, J. Am. Ceram. Soc. 80 (10) (1997) 2563–2568.
[20] J.R. Dygas, F. Krok, W. Boogusz, P. Kurek, K. Reiselhuber, M.W. Breiter, Impedance study of BICUVOX ceramics, Solid State Ionics 70/71 (Part 1) (1994) 239–247.
[21] E. Pernot, M. Anne, M. Bacmann, P. Strobel, Structure and conductivity of Cu and Ni-substituted $Bi_4V_2O_{11}$ compounds, Solid State Ionics 70/71 (Part 1) (1994) 259–263.
[22] P. Kurek, J.R. Dygas, M.W. Breiter, Impedance measurements on single crystals of the oxygen ion conductor BICUVOX, J. Electroanal. Chem. 378 (1994) 77–83.
[23] F. Abraham, J.C. Boivin, G. Mairesse, G. Nowogrocki, The BIMEVOX series: a new family of high performances oxide ion conductors, Solid State Ionics 40/41 (Part 2) (1990) 934–937.
[24] C.K. Lee, G.S. Lim, A.R. West, Phase diagrams and stoichiometries of the solid electrolytes, $Bi_4V_2O_{11}$: M, M=Co, Cu, Zn, Ca,Sr, J. Mater. Chem. 4 (9) (1994) 1441–1444.
[25] S.N. Achary, M.D. Mathews, S.J. Patwe, A.K. Tyagi, High temperature X-ray diffraction and dilatometric studies on some oxygen ion conducting compounds, J. Mater. Sci. Lett. 18 (5) (1999) 355–357.
[26] K. Reiselhuber, G. Dorner, M.W. Breiter, Studies of BICUVOX.10 by conductivity measurement and thermal analysis, Elctrochim. Acta 38 (7) (1993) 969–973.
[27] M. Huve, R.N. Vannier, G. Nowogrocki, G. Mairesse, From $Bi_4V_2O_{11}$ to $Bi_4V_2O_{10.66}$: the V^V–V^{IV} transformation in the aurivillius-type framework, J. Mater. Chem. 6 (8) (1995) 1339–1346.
[28] A.A. Yaremchenko, V.V. Kharton, E.N. Naumovich, A.A. Tonoyan, Stability of δ-Bi_2O_3 based solid electrolytes, Mater. Res. Bull. 35 (2000) 515–520.
[29] B. Jaffe, W.R. Cooke, H. Jaffe, Piezoelectric Ceramics, Academic Press, 1971.

[30] Y, Xu, Ferroelectric materials and their applications, North Holloand, 1991.
[31] J. Yan, M. Greenblatt, Ionic conductivities of $Bi_4V_{2-x}M_xO_{11-x/2}$ (M=Ti, Zr, Sn, Pb) solid solutions, Solid State Ionics 81 (3–4) (1995) 225–233.
[32] C.K. Lee, M.P. Tan, A.R. West, Ge-doped bismuth vanadate solid electrolytes: synthesis, phase diagram and electrical properties, J. Mater. Chem. 4 (1994) 525–528.
[33] F. Krok, I. Abraham, D. Bangobango, W. Bogusz, J.A.G. Nelstrop, Structural and electrical characterization of BINIVOX, Solid State Ionics 111 (1998) 37–43.
[34] I. Abraham, J.A.G. Nelstrop, F. Krok, W. Bogusz, Defect structure of quenched γ-BINIVOX, Solid State Ionics 110 (1998) 95–101.
[35] K.V.R. Prasad, G.N. Subbanna, K.B.R. Varma, Effect of rare earth (Nd & Gd) doping on the structural and dielectric properties of Ferroelectric $Bi_2VO_{5.5}$, Bull. Bismuth Ins. 67 (1994) 3–6.
[36] C.K. Lee, A.R. West, Thermal behaviour and polymorphism of BIMEVOX oxide ion conductors including the new materials: $Bi_4V_2O_{11}$:M; M=La, Y, Mg, B, Solid State Ionics 86–88 (Part 1) (1996) 235–239.